Computers & Geosciences 36 (2010) 871–880

Contents lists available at ScienceDirect

Computers & Geosciences

journal homepage: www.elsevier.com/locate/cageo

A global optimizing approach for waveform inversion of receiver functions ☆

Zhiwei Li [a,*], Tianyao Hao [a], Yi Xu [a], Ya Xu [a], Steve Roecker [b]

[a] Key Laboratory of Petroleum Resources Research, Institute of Geology and Geophysics, Chinese Academy of Sciences, Beijing 100029, China
[b] Department of Earth and Environmental Science, Rensselaer Polytechnic Institute, Troy, New York 12180, USA

ARTICLE INFO

Article history:
Received 26 May 2009
Received in revised form
10 November 2009
Accepted 13 November 2009

Keywords:
Differential evolution
Receiver function
Global optimization
Anisotropy
Seismic structure

ABSTRACT

A global optimizing approach is developed and implemented to retrieve one-dimensional crustal structure by waveform inversion of teleseismic receiver functions. The global optimization for the inversion is performed using a Differential Evolution (DE) algorithm. This modeling approach allows the user to perturb, within a preset range of reasonable bounds, multiple parameters such as V_p, V_p/V_s, thickness and anisotropy of each layer to fit the receiver function waveforms. Compared with linear modeling methods, the global optimal solution can be achieved with fewer model parameters (e.g., a small number of layers) and hence eliminate potential artifacts in the final model. Receiver function bins with small ray parameter intervals are used in the inversion, which can reduce distortion caused by modeling a single receiver function stacked from many recordings spread over a wide range of epicenter distance. The efficacy of this global optimizing approach is demonstrated with synthetic datasets and real receiver functions from the permanent seismic station BJT.

1. Introduction

Teleseismic P-receiver functions contain *P*-to-*S* converted waves (*Ps*) reverberating in the crust and upper mantle beneath a seismic station (Vinnik, 1977; Langston, 1981; Ammon, 1991). They are derived from individual three-component seismograms by decomposition and deconvolution of the radial component from the vertical component. *Ps* converted waves and multiples are sensitive to impedance contrasts and can be used to retrieve the crustal thickness and the average V_p/V_s ratio beneath the station (e.g., Zhu et al., 2006). Full waveform inversion of receiver functions can incorporate multiple converted phases (e.g. *PpPs* and *PpSs+PsPs*,) into the inversion, reducing the non-uniqueness of the resulting model (Zhu et al., 2006). The increasing utilization of temporary broadband arrays in recent years has resulted in a number of investigations that use receiver function waveform inversion to determine *S*-wave velocity, V_p/V_s ratio, thickness of the crust (Owens, 1987; Kosarev et al., 1993; Wu and Zeng, 1998; Roecker, 2001; Kim et al., 2004; Vinnik et al., 2004; Zheng et al., 2005), and even the anisotropic structure and layer dip (Levin et al., 2002, 2008; Frederiksen et al., 2003).

Despite its popularity, receiver function waveform modeling is a highly non-linear and non-unique inverse problem (e.g., Ammon et al., 1990; Sambridge, 1999; Frederiksen et al., 2003). Although crustal models derived from linearized, iterative, and gradient-based approaches may fit the observed receiver function waveforms very well, the solution usually suffers from a strong dependence on the starting model, and can often converge to a local (as opposed to global) optimal solution. The linearized approach becomes much more complex when V_p/V_s and anisotropy are added as parameters. Moreover, there are often too many variables (e.g., too many layers) in the models derived from linear inversion techniques, which can create artifacts. In contrast, Monte Carlo techniques, such as the simulated annealing algorithm, can avoid local minima and achieve the global optimal solution with a small number of model parameters. Additionally, more parameters (e.g. V_p/V_s and anisotropy) can be introduced into the inversion without overly complicating the procedure. Monte Carlo techniques have proved very successful in receiver function waveform inversion (Sambridge, 1999; Vinnik et al., 2004; Zheng et al., 2005). At the same time, many of these studies interpret a single receiver function obtained from stacking many records with different ray parameters. Due to the limited moveout in teleseismic receiver functions, a stacking can increase the ambiguity of the model (e.g., Frederiksen et al., 2003). Modeling receiver functions stacked in small bins of ray parameter intervals (e.g. 0.004 s/km) can largely remove the limitations caused by a moveout correction. A scheme with multiple bins of receiver functions can also be applied to inversion for anisotropic structure, which requires receiver functions with different back-azimuths (Levin et al., 1997a, 2002, 2008, Frederiksen et al., 2003).

In this paper, we adapt a simple and efficient scheme for global optimization–the Differential Evolution (DE) algorithm (Storn and Price, 1997), to receiver function waveform inversion. We note that receiver function inversion shares many of the generic

☆ Code available from server at http://www.iamg.org/CGEditor/index.htm

* Corresponding author.
E-mail address: zwli@mail.iggcas.ac.cn (Z. Li).

0098-3004/$ - see front matter © 2010 Elsevier Ltd. All rights reserved.
doi:10.1016/j.cageo.2009.11.007

difficulties of waveform inversion (Sambridge, 1999); therefore, we can meaningfully extend the application of the DE algorithm to general non-linear waveform inversion. In the following sections, we first discuss the waveform inversion for isotropic and anisotropic crustal structure with synthetic receiver functions to establish the validity of our approach. We then apply this approach to real receiver functions from a permanent seismic station near Beijing (BJT) to retrieve an estimate of the isotropic crustal structure beneath the station. We try different strategies during the inversions to reduce the non-uniqueness of the waveform inversion and obtain robust results by setting reasonable ranges for unknown parameters.

Table 1
Models used to test the recovery of isotropic parameters using synthetic datasets. Depth shows the bottom of each layer. V_s is calculated through V_p and fixed V_p/V_s. ρ is calculated through the relationship between V_p and density by the empirical equations (Roecker et al., 2004). The depth and V_p of each layer are chosen to vary in a preset scale (Fig. 1 for model A and Fig. 2 for model B).

[a]Depth (km)	[a]V_p (km/s)	V_s (km/s)	V_p/V_s	ρ (g/cm^3)
Synthetic model A				
5.0	5.50	3.24	1.70	2.67
15.0	6.20	3.58	1.73	2.78
25.0	6.30	3.64	1.73	2.81
40.0	6.60	3.77	1.75	2.90
100.0	8.00	4.44	1.80	3.30
Recovered model A (with noise-free data)				
5.0	5.52	3.25	1.70	2.67
14.4	6.25	3.61	1.73	2.80
24.9	6.33	3.66	1.73	2.82
40.0	6.62	3.78	1.75	2.90
100.0	8.00	4.44	1.80	3.30
Recovered model A (with noisy data)				
7.8	5.68	3.34	1.70	2.67
14.9	6.23	3.61	1.73	2.79
23.4	6.59	3.81	1.73	2.89
40.5	6.55	3.74	1.75	2.88
100.0	8.00	4.44	1.80	3.30
Synthetic model B				
5.0	5.50	3.24	1.70	2.67
15.0	6.20	3.58	1.73	2.78
25.0	6.00	3.47	1.73	2.72
40.0	6.60	3.77	1.75	2.90
100.0	8.00	4.44	1.80	3.30
Recovered model B (with noise-free data)				
5.0	5.50	3.24	1.70	2.67
14.4	6.20	3.58	1.73	2.78
24.9	5.99	3.46	1.73	2.72
40.0	6.59	3.77	1.75	2.89
100.0	8.00	4.44	1.80	3.30
Recovered model B (with noisy data)				
0.1	6.20	3.24	1.70	2.78
11.5	6.27	3.58	1.73	2.80
25.2	5.90	3.46	1.73	2.70
40.4	6.59	3.77	1.75	2.89
100.0	8.00	4.44	1.80	3.30

[a] Depth (i.e., layer thickness) and V_p are the parameters allowed to vary.

2. Methodology

2.1. Receiver function forward modeling and stacking

We employ the reflectivity technique for one-dimensional horizontally stratified anisotropic media (Levin and Park, 1997a, 1997b, 1998) to generate synthetic receiver functions, as this technique may be easily adapted to global optimal receiver function waveform inversion. We use the maximum entropy deconvolution method (Wu and Zeng, 1998), to isolate radial and transverse receiver functions from three-component waveforms, which is effective and stable for receiver function calculations (Zheng et al., 2005). Receiver functions are binned according to ray parameter at small intervals (0.004 s/km) for isotropic inversion. For anisotropic inversions, both ray parameter and back-azimuth are binned with small intervals (0.004 s/km and 10 degrees, respectively). As discussed above, a moveout correction is not necessary for such small ray parameter intervals.

2.2. Differential evolution algorithm

As a type of evolutionary technique analogous to genetic algorithms, DE is well suited to highly non-linear, multi-parameter objective functions (Storn and Price, 1997). DE includes mutation, crossover, and selection operators, but generates a new population vector from a weighted difference vector between two randomly selected population vectors. A newly generated vector with a smaller objective function will replace the vector with larger objective functions in the next generation. The population vector with the minimum objective function is retained until all iterations are finished.

Some of the important control variables that can be adjusted for an individual inversion problem include the number of generations (G), the number of parameter vectors (Np) as a population for each generation G, a factor (F) which controls the amplification of

Table 2
Models used to test the recovery of the anisotropic model C. The anisotropy coefficients B and E indicate the peak-to-peak variations of V_p and V_s, respectively. The angles of θ and φ represent the inclination (from vertical) and the strike (CW from north) of the axis of symmetry within each anisotropic layer (Levin, et al., 2002). The scales for searching θ and φ are 0–180 degree and 0–360 degree, respectively.

[a]Depth (km)	[a]V_p (km/s)	[a]B (% of V_p)	V_s (km/s)	V_p/V_s	ρ (g/cm^3)	[a]E (% of V_s)	[a]θ (degree)	[a]φ (degree)
Synthetic model C								
20.0	6.20	8.0	3.58	1.73	2.78	8.0	45	45
40.0	6.60	8.0	3.77	1.75	2.90	8.0	60	90
100	8.00	–	4.44	1.80	3.30	–	–	–
Recovered model C (with noise-free data)								
19.8	6.16	7.9	3.56	1.73	2.77	7.9	44	45
39.6	6.58	7.9	3.76	1.75	2.89	7.9	60 (120)[b]	90 (270)[b]
100	8.00	–	4.44	1.80	3.30	–	–	–
Recovered model C (with noise data)								
20.6	6.37	8.6	3.68	1.73	2.83	8.6	39	44
40.5	6.60	8.2	3.77	1.75	2.90	8.2	64	87
100	7.91	–	4.39	1.80	3.30	–	–	–

[a] Depth (i.e., layer thickness), V_p, B, E, θ and φ are the parameters allowed to vary (Note that B and E are adjusted synchronously).
[b] θ and φ in the parentheses are the result from inversion, which depict the same anisotropic property as θ and φ outside the parentheses.

differential variations between two vectors, and the crossover probability *(Cr)*. Based on previous studies (Storn and Price, 1997; Růžek and Kvasnička, 2001, 2005; Li et al., 2006) and our tests, we determined the following criteria to be appropriate for receiver function inversion: *Np* should be between 5 and 20 times the number of unknown parameters, *F* should be as large as 0.8 to prevent the population from converging prematurely and *Cr* should be as large as 0.9 for fast convergence.

DE is much more efficient than pure Monte Carlo random search techniques, and has been successfully used in classic non-linear geophysical inversion problems such as earthquake hypocenter location and arrival time tomography (Růžek and Kvasnička, 2001, 2005; Li et al., 2006). These applications demonstrate the usefulness of DE in solving non-linear inversion problems. Below we describe an application of DE to waveform inversion.

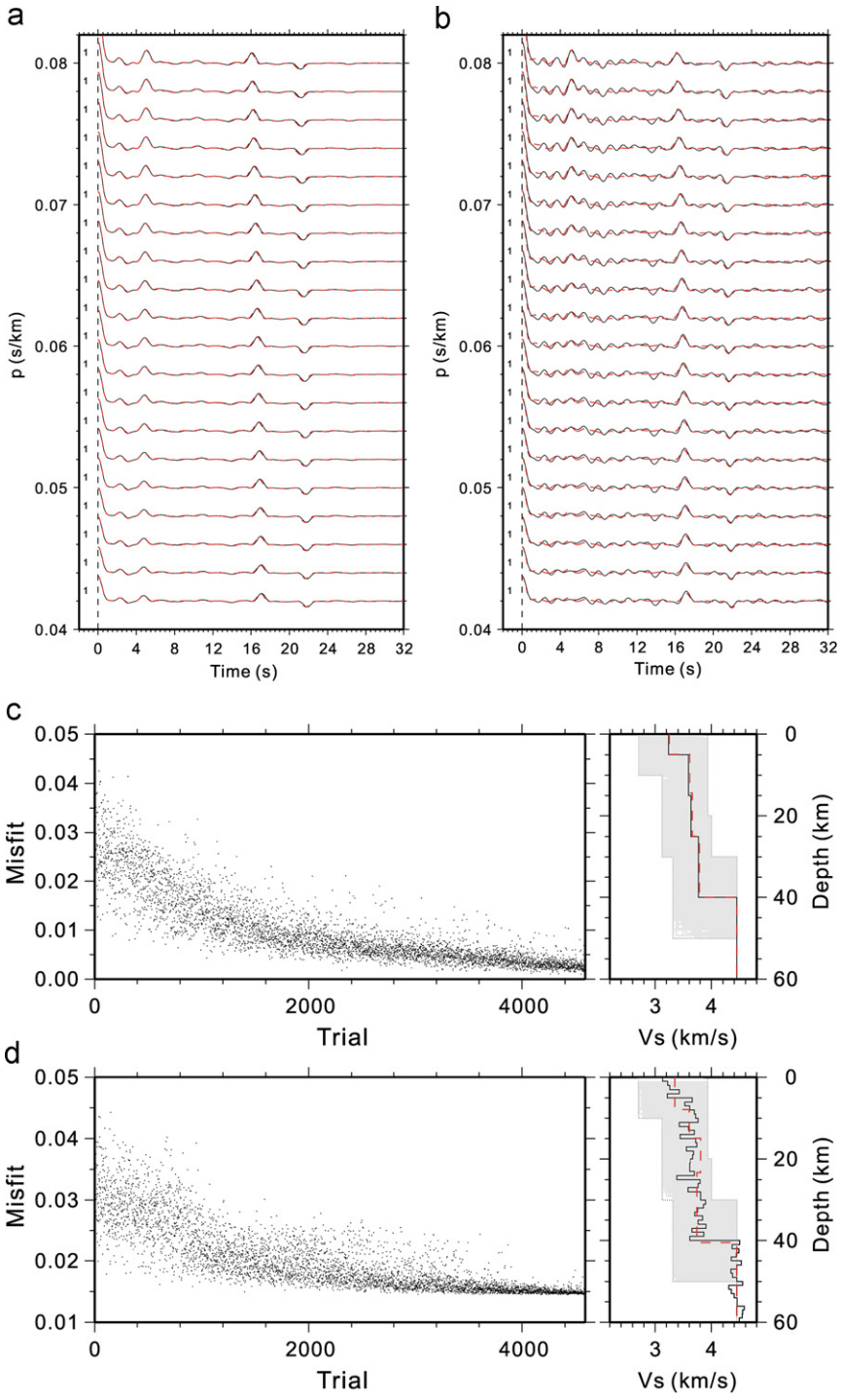

Fig. 1. Synthetic tests for isotropic model A: (a) synthetic (solid line) and recovered (dashed line) radial receiver functions for noise-free datasets. Number on left side of each waveform indicates number of receiver functions in this bin; (b) similar figure to Fig. 1a but for datasets with noise; (c) left panel shows objective function decreasing with iteration increasing, while right panel shows synthetic (solid line) and recovered (dashed line) *S*-wave velocity models for noise-free data. Dotted lines show lower and upper boundaries for *S*-wave velocity searching ranges; gray regions inside lower and upper boundaries show plots for all possible *S*-wave velocity models in global optimum searching and (d) similar figure to Fig. 1c but for datasets with noise.

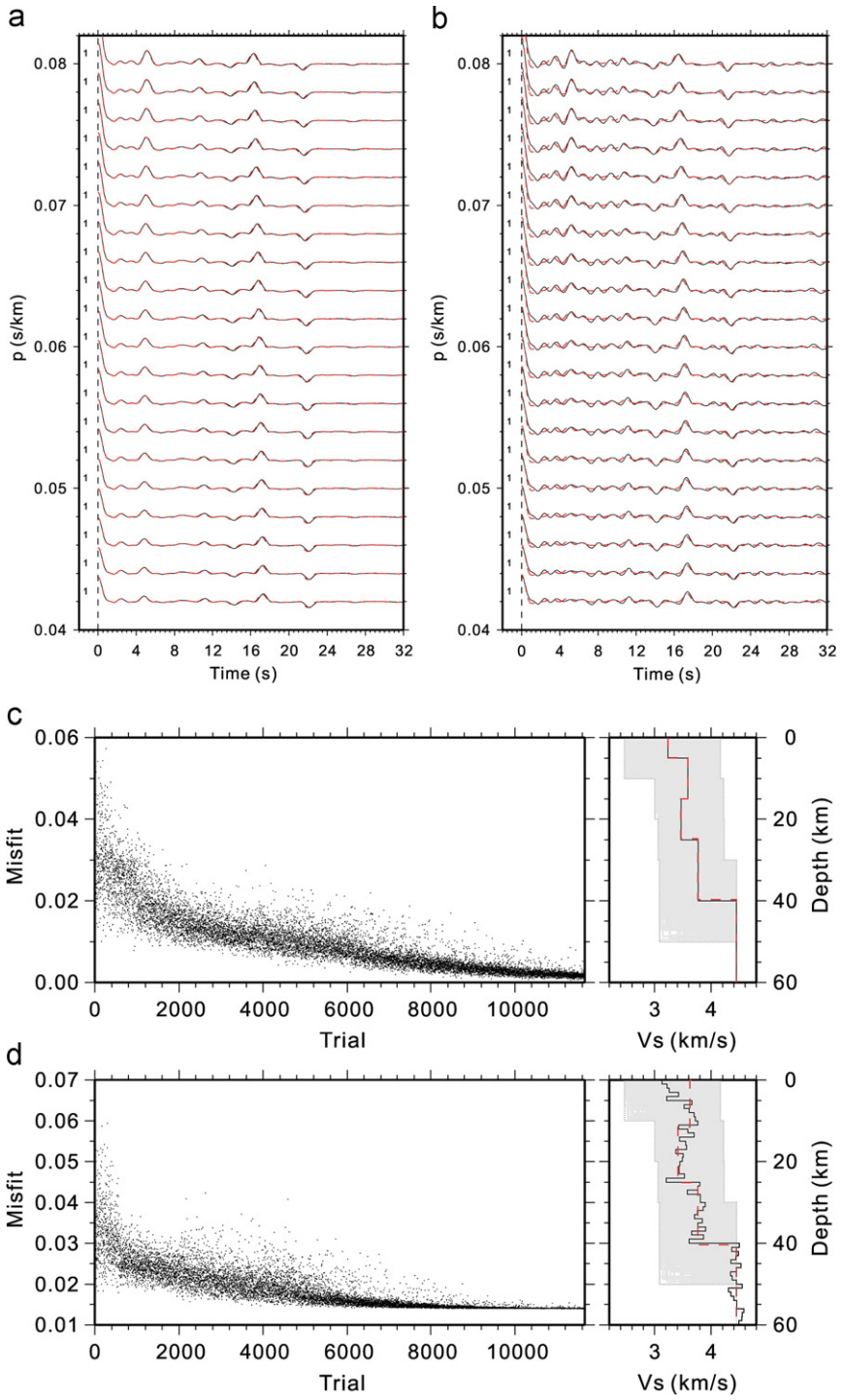

Fig. 2. Similar figure to Fig. 1 but for isotropic model B.

2.3. Objective function

To model receiver functions, radial and transverse receiver functions are first computed for trial models and ray parameters. We adopt an objective function $E(m)$ to quantify the misfit between observed and calculated receiver functions

$$E(m)=\alpha\sum_{i=1}^{N_b}\frac{n_i}{N}\left\|O_{iR}(t)-S_{iR}(t)\right\|+(1-\alpha)\sum_{j=1}^{M_b}\frac{m_j}{M}\left\|O_{jT}(t)-S_{jT}(t)\right\| \quad (1)$$

where $O_{iR}(t)$ and $O_{jT}(t)$ are the observed ith and jth bins of radial and transverse receiver functions; $S_{iR}(t)$ and $S_{jT}(t)$ are the calculated radial and transverse receiver functions with the same ray parameter (and back-azimuth for anisotropic inversion) as the ith and jth bins of observed data; n_i and m_j are the trace numbers

Table 3
Control parameters of DE used in the tests. D includes the V_p of the bottom layer in the isotropic or anisotropic model.

	D	Np	Cr	F	G
Synthetic model A	9	16∗D	0.98	0.86	80
Synthetic model B	9	16∗D	0.98	0.86	80
Synthetic model C	9	16∗D	0.98	0.86	100

of radial and transverse receiver functions for the ith and jth bins of ray parameters (and back-azimuth for anisotropic inversion), respectively; N_b and M_b are the numbers of bins for radial and transverse receiver functions, respectively; N and M are the trace numbers of all radial and transverse receiver functions used in the inversion, respectively. The factor α weights the relative contributions of radial and transverse components and is set to 1 for isotropic media. For anisotropic media, α is usually set to be less than 0.5 because the amplitudes of transverse components are generally smaller than the radial.

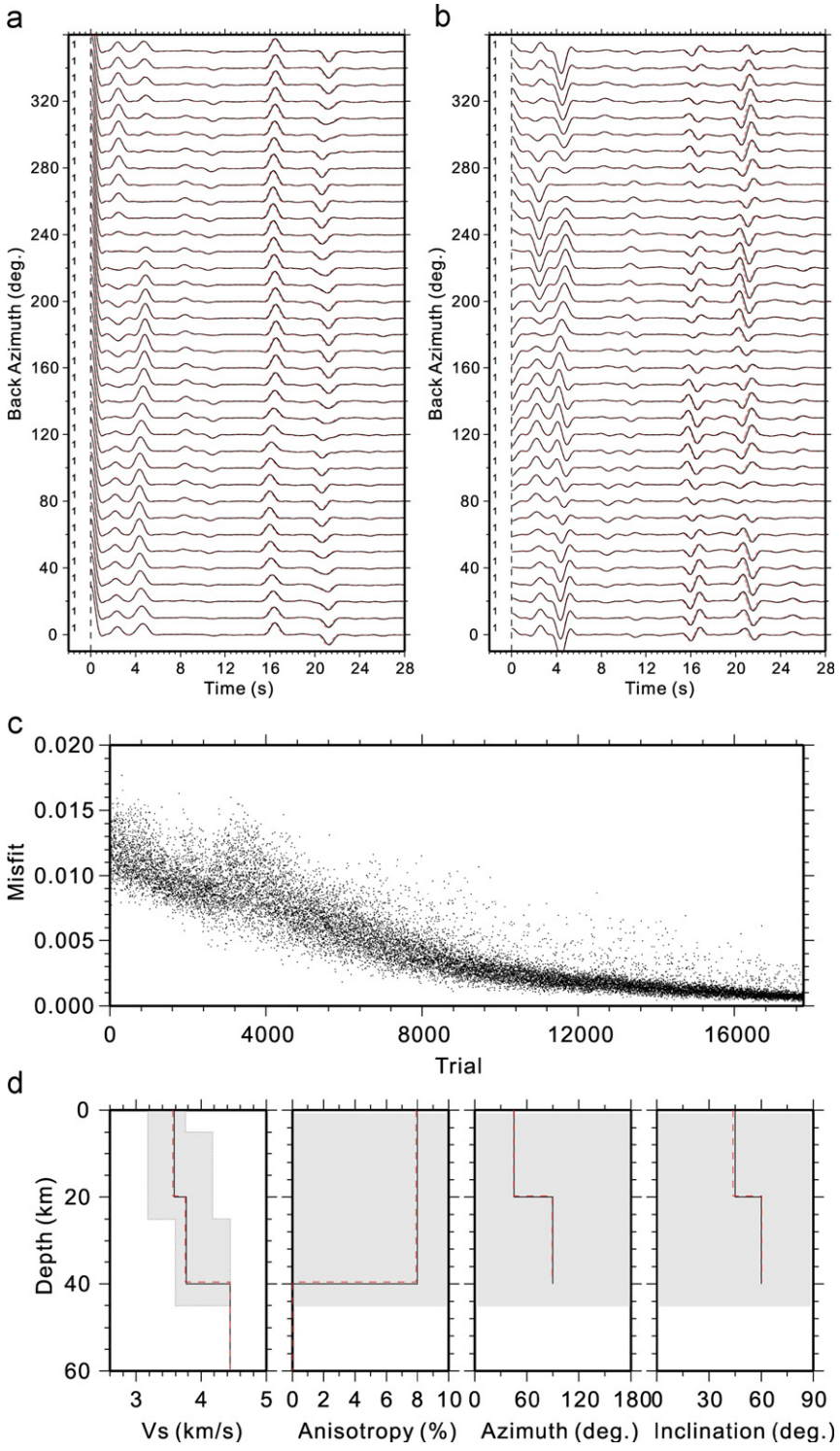

Fig. 3. Synthetic tests for anisotropic model C with noise-free datasets: (a) synthetic (solid line) and recovered (dashed line) receivers for radial components; (b) similar figure to Fig. 3a but for transverse receiver functions. Compared with radial receiver functions, transverse components are zoomed 2 times due to their smaller amplitude than radial ones; (c) objective functions are decreasing with iteration increasing and (d) V_s, peak-to-peak anisotropic variations of V_p and V_s, the strike (CW from north) and inclination (from vertical) of the axis of symmetry for synthetic (solid line) and recovered (dashed line) models, respectively. Gray regions show plots for all possible parameters in global optimum searching.

A similar objective function was used successfully by Vinnik et al. (2004). Given the relatively high signal-to-noise ratio (SNR) of real receiver functions at station BJT, the objective function of Eq. (1) works well in this study. We note that other types of objective functions (e.g., cross-correlation coefficient) might be more advantageous when receiver functions with low SNR are analyzed, but also that other objective functions can easily be integrated into the DE approach.

3. Evaluation and application

In this section, we use synthetic and real receiver functions to evaluate the DE global optimizing approach for waveform inversion. In principle, the thickness, V_p, V_p/V_s, anisotropy (including inclination and strike of the axis of symmetry and anisotropic strength) of each layer in the one-dimensional models may be specified as parameters for inversion. In practice however,

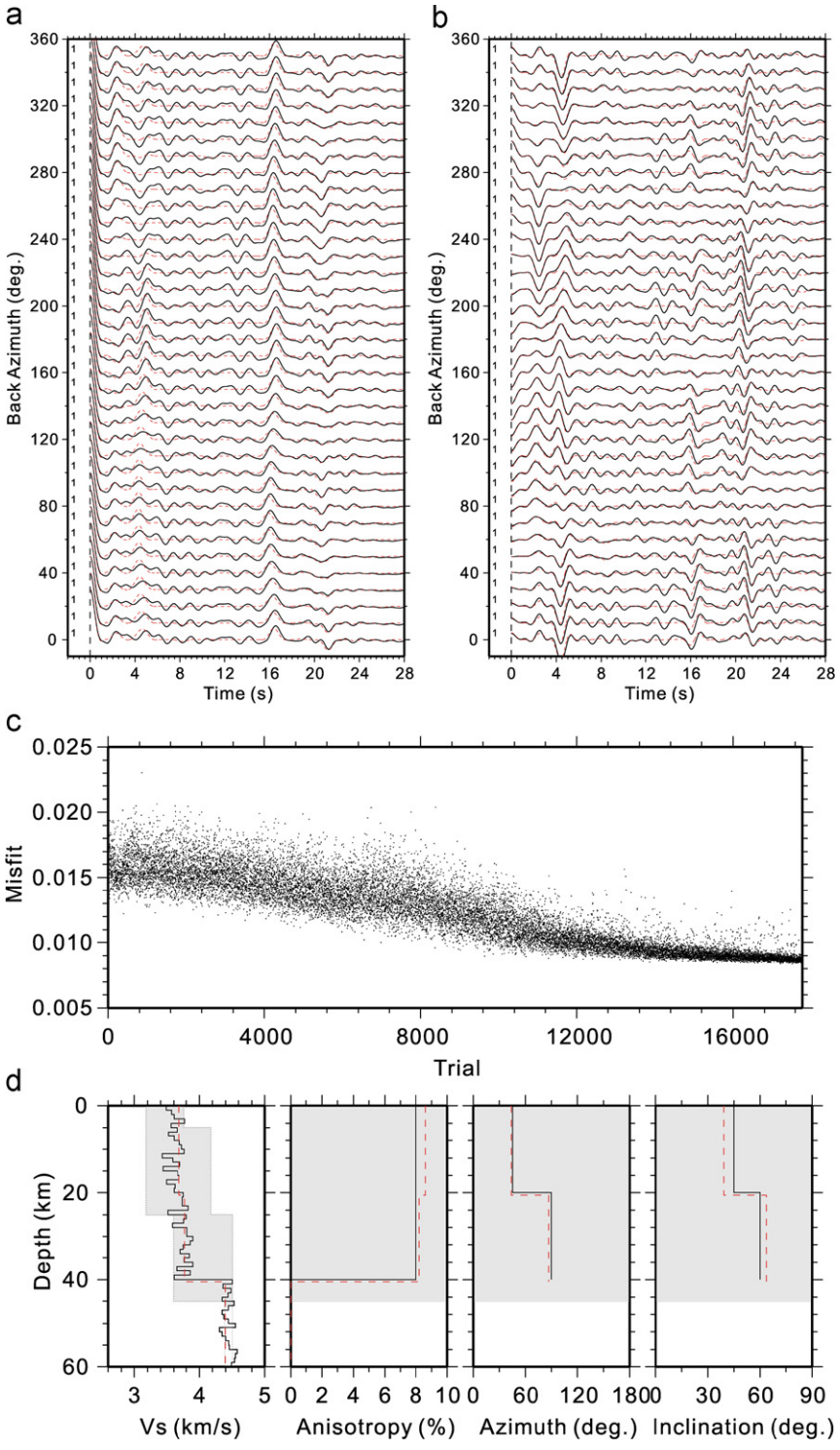

Fig. 4. Similar figure to Fig. 3 but for synthetic datasets with noise.

because of trade-offs among these parameters, V_p and layer thicknesses generally are chosen to be unknowns, while the V_p/V_s ratio typically is fixed, and the anisotropic strengths of V_p and V_s are assumed to be the same for anisotropic inversion (Levin et al., 2008). Once the number of layers is determined, then V_p, thickness, and anisotropic parameters of each layer can be adjusted within specified ranges to fit observed receiver functions. V_s of each layer can be calculated directly through V_p and fixed V_p/V_s. The number of layers can be determined through a trial-and-error process based on receiver function fits and prior knowledge of crustal structure. Generally, a model with a large number of layers can fit the observed data well, but is also sensitive to the noise and may include significant artifacts. Therefore, the models used in the synthetic and real inversions discussed below generally consist of only a few layers which still can characterize the actual structures.

3.1. Synthetic receiver function tests

We constructed two four-layer isotropic models (model A and B, shown in Table 1) and one two-layer anisotropic model (model C, shown in Table 2) to test our approach. Model A represents a normal crustal structure with positive velocity gradient, while model B represents a crust with a low velocity layer in the middle-lower crust. Model C consists of two layers in the crust with different anisotropic properties.

Synthetic data for the isotropic models consist of 20 radial receiver functions with ray parameters ranging from 0.042 to 0.08 s/km at 0.002 s/km intervals. The synthetic data for the anisotropic model consist of 36 radial and transverse receiver functions with back azimuth ranging from 0 to 350 degrees at 10 degrees intervals and ray parameters are all set to 0.06 s/km for simplicity. A Gaussian filter of 2.5 Hz (approximately 1.2 Hz

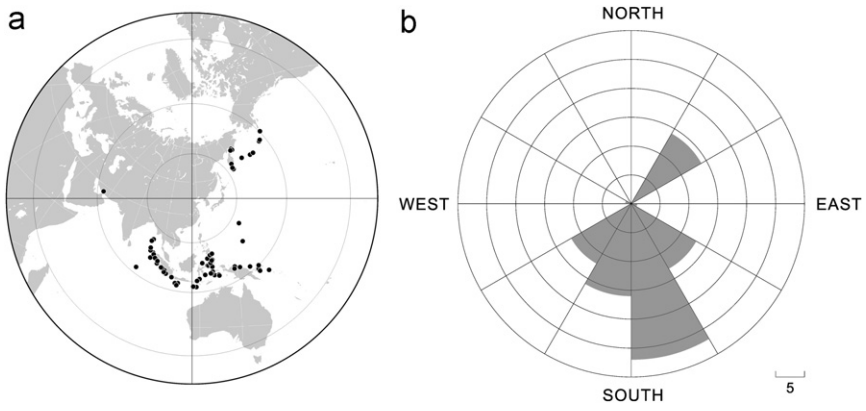

Fig. 5. (a) Map of teleseismic events used to generate receiver function dataset for inversion. Events are plotted as black dots on an azimuthal equidistant projection centered on station BJT. Concentric circles are plotted in increments of 3000 km from center and (b) Back-azimuth distribution of teleseismic events. Note that most of events are distributed to southeast and southwest of station BJT.

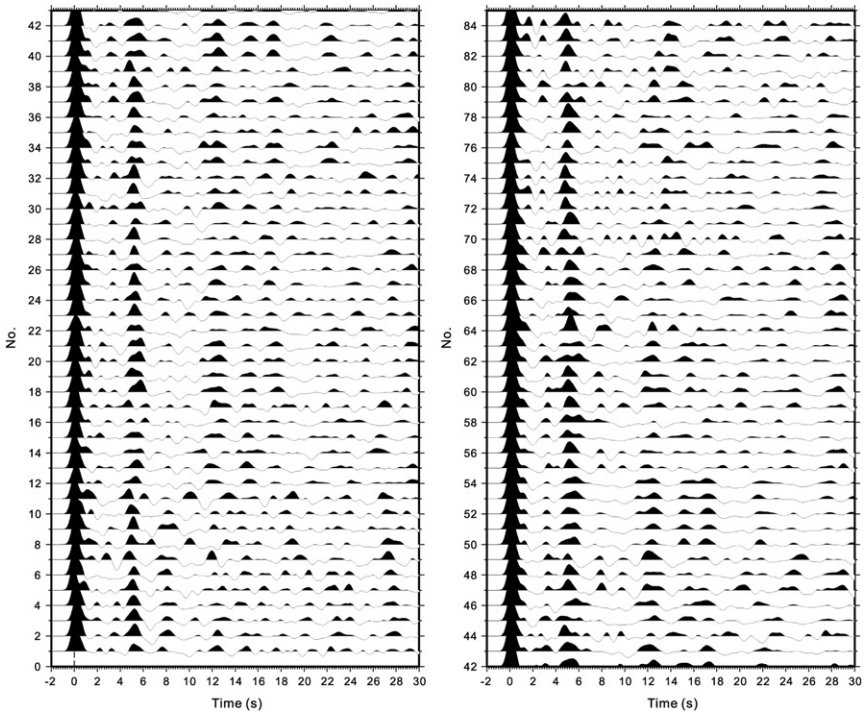

Fig. 6. Radial receiver functions for station BJT. Receiver functions are sorted by ray parameters (ray parameters are increasing with the No. of receiver functions). A common amplitude scale is adopted for all plots.

maximum frequency) is applied in the forward calculations. A time window of 32 s after the P arrival is used so that both direct and multiple mode conversions are included in the inversion. Synthetic datasets with and without noise are used in the tests. Noise-free receiver functions are calculated based on the synthetic models directly. Noisy receiver functions are generated by first subdividing each layer in the medium into 1 km thick intervals and then perturbing the V_p of each thin layer by random Gaussian noise. Perturbations are zero mean with standard deviations of 0.2 and 0.1 km/s, respectively, above and below 50 km depth. We note that randomly perturbing the input model can generate coherent noise, and provides a useful way to evaluate the ability of our approach to resolve the main characteristics of a complex model with only a few layers.

With noise-free datasets, the recovered models and waveforms for both A and B (Figs. 1 and 2) are very close to the synthetics. With the datasets from randomly perturbed models, the recovered models with fewer layers still could reflect the main characteristics of synthetic models with many thin layers.

In inverting for model C (Table 2) we set the weight factor α to 0.25 to compensate the smaller amplitudes in the transverse components (a complete summary of control parameters we used is shown in Table 3). As in the isotropic case, both the waveforms and models are well fit for synthetic datasets with and without noise (Figs. 3 and 4). This test demonstrates that DE can work well in an anisotropic environment, although one can expect that more observations (both radial and transverse receiver functions) and good back-azimuth coverage will be necessary for a reasonable anisotropic inversion.

The synthetic receiver function inversions described here required about 10^4 forward calculations to guarantee a global optimum solution, but fortunately the forward calculation of receiver functions is very efficient. The actual computational load will depend on model complexity and the size of the allowable bounds for the parameters, but, to give an example, a 2.66 GHz Xeon CPU can find a global optimum solution for a problem the size of our synthetic examples in about 4 h.

Table 4
Best-fitting crustal model beneath the station BJT.

[a]Depth (km)	[a]V_p (km/s)	V_s (km/s)	V_p/V_s	ρ (g/cm^3)
2.0	4.89	2.83	1.73	2.59
12.0	6.01	3.47	1.73	2.73
30.2	6.58	3.80	1.73	2.89
40.7	7.17	4.14	1.73	3.06
100.0	7.90	4.44	1.80	3.30

[a] Depth (i.e., layer thickness) and V_p are the parameters allowed to vary.

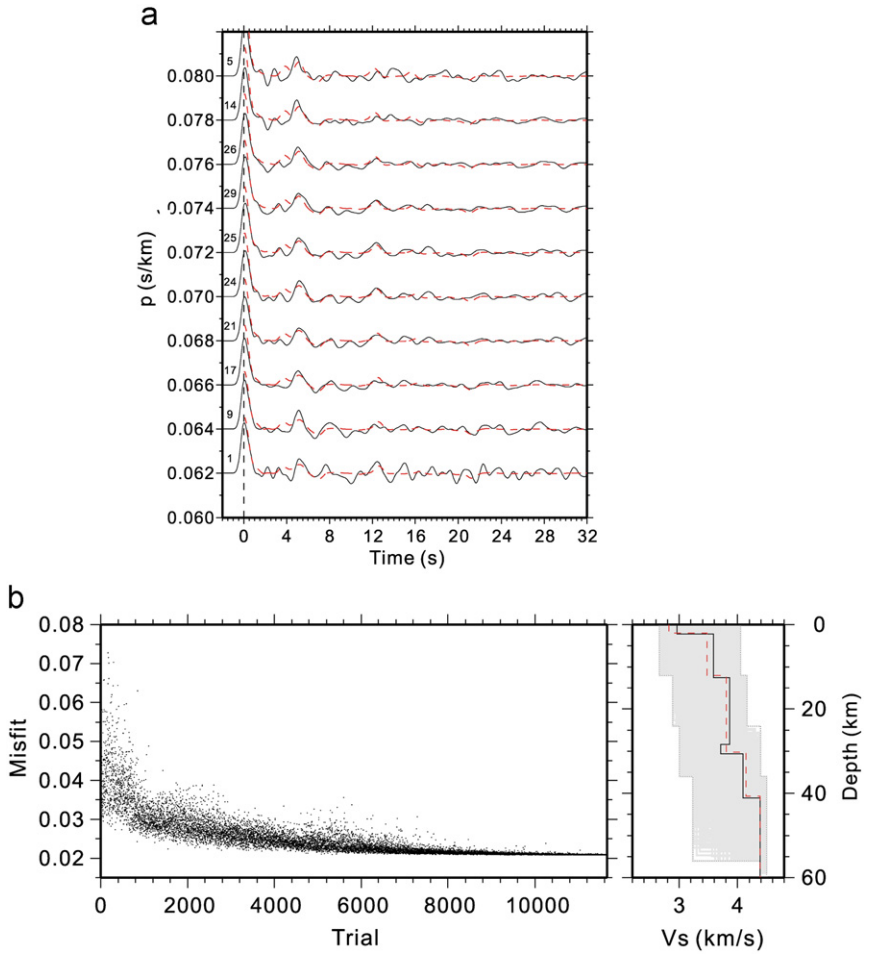

Fig. 7. *S*-wave velocity model inversion for station BJT: (a) observed (solid line) and recovered (dashed line) radial receivers and (b) left panel shows objective functions for four-layer model inversion, while right panel shows recovered five-layer (solid line) and four-layer (dashed line) *S*-wave velocity models. Dotted lines show lower and upper boundaries for *S*-wave velocity searching ranges; gray regions inside lower and upper boundaries show plots for all possible *S*-wave velocity models in global optimum searching. Note that main characteristics of five-layer and four-layer models are almost the same.

3.2. Application to receiver functions at station BJT

As an example of an application using real data, we analyzed records from station BJT, located near Beijing (Fig. 5). The crustal structure in this region is well sampled by teleseisms recorded by dense deployments of permanent and temporary stations (Liu et al., 1997; Wang et al., 2009). The seismic dataset we use consists of 290 teleseismic events recorded in 2006 and 2007, with epicenter distances ranging from 30 to 90 degrees (Fig. 5). A Gaussian filter of 2.5 Hz (approximately corresponding to a maximum frequency of 1.2 Hz) is adopted in the deconvolution to generate the radial and transverse receiver functions. After deconvolution, 101 receiver functions with high signal-to-noise ratios are selected to conduct the inversion (Fig. 6). We selected those receiver functions with ray parameters larger than 0.06 s/km as nearly all of the high quality waveforms are in this set, and binned them in 0.004 s/km overlapping intervals at 0.002 s/km spacing, so that each receiver function influences two adjacent bins. Due to the uneven azimuthal distribution of teleseismic events (Fig. 5b), reliable anisotropic structures are difficult to retrieve with this dataset and so we invert only for isotropic crustal structure.

A time window of 24 s after the P arrival is used to calculate the objective function, which will include both the main *Ps* conversions and all the principal multiples relevant to crustal structure. Our choices for *Np*, *Cr*, and *F* are the same as those shown in Table 3 for models A and B, and the number of unknown parameters *D* is 9 for a four-layer model. These parameters are sufficient to achieve convergence for the inversion of an isotropic model with a small number of layers. According to previous studies near station BJT (Liu et al., 1997; Wang et al., 2009), a crustal model with only a few layers should be sufficient to characterize the main features of the crust. We tested several models with different numbers of layers, and find that a 4-layer model could fit the observations nearly as well as a 5-layer model, and moreover that the models themselves are quite similar (Fig. 7). We also found that models with fewer than 4 layers result in a significantly poorer fit to the observations.

The *Ps* conversions and main multiples of observed and recovered receiver functions in the 4-layer model coincide very well and the prominent characteristics of crustal structure (shown in Table 4 and Fig. 7) are similar to those found in previous studies (Liu et al., 1997; Wang et al., 2009). We obtained a crustal thickness of about 40.7 km, which is very close to the result of 39.8 km obtained from receiver function study of the nearby temporary broadband station LQS (E116.07, N40.11) (Wang et al., 2009).

4. Conclusions

We have developed an approach for receiver function waveform inversion based on the DE global optimal algorithm. The results of inversions with synthetic and real dataset demonstrate that the DE approach is capable of retrieving both isotropic and anisotropic structures. An advantage of the DE algorithm is that it avoids linearization of the inversion problem and hence is capable of obtaining the global optimal solution. Of course, the global optimal approach for non-linear inversion requires a large number of forward calculations to guarantee that convergence is achieved.

The approach described in this paper is also very flexible. Parameters such as the thickness, V_p, V_p/V_s, and anisotropic structures of each layer, can be fixed or variable. However, the thickness and V_p of each layer generally are chosen in the inversion due to the trade-off between V_p/V_s and thickness of layers, while V_s could be calculated directly from V_p and V_p/V_s. Different types of objective functions can be implemented into the approach easily to accommodate different qualities of observed datasets. The ray parameter intervals of receiver function bins can also be adjusted according to need. The disadvantages of global optimal techniques are the potentially large number of computations, especially when many of layers and anisotropic parameters are involved in the inversion. Inherent trade-offs and ambiguities between different parameters can also complicate the inversion, but DE does allow for a convenient way to apply Occam's razor to receiver function analysis.

Acknowledgments

We are grateful to Prof. V. Levin, Prof. J. Park and Prof. Wu Q.J. for making their receiver function forward codes available. Li Z. wishes to thank Dr. Liu J.S. and Dr. Zhang L.L. for their helps. We greatly thank two anonymous reviewers and the Editor-in-Chief, Eric Grunsky, for improving the manuscript significantly. The seismic waveforms of station BJT are obtained from the IRIS. This study was supported by the National Natural Science Foundation of China (90814011, 40620140435, 40804016, and 40704013) and the National Basic Research Program of China (2007CB411701).

References

Ammon, C.J., 1991. The isolation of receiver function effects from teleseismic P waveforms. Bulletin of Seismology Society of America 81, 2504–2510.
Ammon, C.J., Randall, G.E., Zandt, G., 1990. On the non-uniqueness of receiver function inversions. Journal of Geophysical Research 95, 15303–15318.
Frederiksen, A.W., Folsom, H., Zandt, G., 2003. Neighbourhood inversion of teleseismic Ps conversions for anisotropy and layer dip. Geophysical Journal International 155, 200–212.
Kim, K.H., Chiu, J.M., Kao, H., Liu, Q.Y., Yeh, Y.H., 2004. A preliminary study of crustal structure in Taiwan region using receiver function analysis. Geophysical Journal International 1159, 146–164.
Kosarev, G.L., Petersen, N.V., Viniik, L.P., Roecker, S.W., 1993. Receiver functions for the Tien Shan analog broad-band network: contrasts in the evolution of structures across the Talas-Fergana fault. Journal of Geophysics Research 98, 4437–4448.
Langston, C.A., 1981. Structure under Mount Rainier, Washington, inferred from teleseismic body waves. Journal of Geophysical Research 84, 4749–4762.
Levin, V., Park, J., 1997a. Crustal anisotropy in the Ural Mountains foredeep from teleseismic receiver functions. Geophysical Research Letters 24, 1283–1286.
Levin, V., Park, J., 1997b. P-SH conversions in a flat-layered medium with anisotropy of arbitrary orientation. Geophysical Journal International 131, 253–266.
Levin, V., Park, J., 1998. A P-SH conversion in a layered media with hexagonally symmetric anisotropy: a cookbook. Pure and Applied Geophysics 151, 669–697.
Levin, V., Park, J., Brandon, M., Lees, J., Peyton, V., Gordeev, E., Ozerov, A., 2002. Crust and upper mantle of Kamchatka from teleseismic receiver functions. Tectonophysics 358, 233–265.
Levin, V., Roecker, S., Graham, P., Hosseini, A., 2008. Seismic anisotropy indicators in western Tibet: shear wave splitting and receiver function analysis. Tectonophysics 462, 99–108.
Li, Z.W., Xu, Y., Hao, T.Y., Liu, J.S., Zhang, L., 2006. Inversion of crustal velocity model and earthquake relocation by using differential evolution algorithm. Progress in Geophysics 21 (2), 370–378.
Liu, Q.Y., Li, S.C., Shen, Y., Chen, J.H., 1997. Broadband seismic array study of the crust and upper mantle velocity structure beneath Yanhuai Basin and its neighboring region. Chinese Journal of Geophysics 40 (6), 763–772.
Owens, T.J., 1987. Crustal structure of the Adirondacks determined from broadband teleseismic waveform modeling. Journal of Geophysical Research 92, 6391–6401.
Roecker, S., 2001. Constraints on the crust and upper mantle of the Kyrgyz Tien Shan from the preliminary analysis of GHENGIS broadband data. Russian Geology and Geophysics 42, 1554–1565.
Roecker, S., Thurber, C., McPhee, D., 2004. Joint inversion of gravity and arrival time data from Parkfield: new constraints on structure and hypocenter locations near the SAFOD drill site. Geophysical Research Letters 31, L12S04, doi:10.1029/2003GL019396.
Růžek, B., Kvasnička, M., 2001. Differential evolution algorithm in the earthquake hypocenter location. Pure and Applied Geophysics 158, 667–693.
Růžek, B., Kvasnička, M., 2005. Earthquake hypocenter location: a challenge for the differential evolution algorithm. In: Price, K., Storn, R., Lampinen, J. (Eds.),

Differential Evolution, A Practical Approach to Global Optimization. Springer-Verlag, Berlin, pp. 379–392.
Sambridge, M., 1999. Geophysical inversion with a neighbourhood algorithm-I. Searching a parameter space. Geophysical Journal International 138, 479–494.
Storn, R., Price, K., 1997. Differential Evolution—a simple and efficient heuristic for global optimization over continuous spaces. Journal of Global Optimization 11, 341–354.
Vinnik, L., 1977. Detection of waves converted from P to SV in the mantle. Physics of the Earth and Planetary Interiors 15, 39–45.
Vinnik, Lev P., Regber, C., Aleshin, I.M., Kosarev, G.L., Kaban, M.K., Oreshin, S.I., Roecker, S.W., 2004. Receiver function tomography of the central Tien Shan. Earth Planetary Science Letter 225, 131–146.
Wang, J., Liu, Q.Y., Chen, J.H., Li, S.C., Guo, B., Li, Y., 2009. The crustal thickness and Poisson's ratio beneath the capital circle region. Chinese Journal of Geophysics 52 (1), 57–66.
Wu, Q.J., Zeng, R.S., 1998. The crustal structure of Qinghai-Xizang plateau inferred from broadband teleseismic waveform. Chinese Journal of Geophysics 41, 669–679.
Zheng, T.Y., Zhao, L., Chen, L., 2005. A detailed receiver function image of the sedimentary structure in the Bohai Bay Basin. Physics of the Earth and Planetary Interiors 152, 129–143.
Zhu, L., Mitchell, B.J., Akyol, N., Kekovali, K., 2006. Crustal thickness variations in the Aegean region and implications for the extension of continental crust. Journal of Geophysics Research 111, B01301, doi:10.1029/2005JB003770.